Journal of Catalysis 352 (2017) 229–238

Contents lists available at ScienceDirect

Journal of Catalysis

journal homepage: www.elsevier.com/locate/jcat

Highly efficient asymmetric epoxidation of olefins with a chiral manganese-porphyrin covalently bound to mesoporous SBA-15: Support effect

Afsaneh Farokhi, Hassan Hosseini Monfared *

Department of Chemistry, University of Zanjan, 45195-313 Zanjan, Islamic Republic of Iran

ARTICLE INFO

Article history:
Received 2 March 2017
Revised 19 May 2017
Accepted 22 May 2017

Keywords:
Manganese(III)-porphyrin
Enantioselectivity
Heterogeneous catalysis
Oxidation
Mesoporous

ABSTRACT

A chiral Mn^{III}-porphyrin complex covalently bonded with mesoporous SBA-15 (SBA15-[Mn(TCPP-R*)Cl]) was synthesized and fully characterized. The heterogeneous SBA15-[Mn(TCPP-R*)Cl] exhibited remarkable catalytic activity toward enantioselective olefin epoxidation using O_2 as terminal oxidant in the presence of isobutyraldehyde. The catalyst showed higher enantioselectivity than its homogeneous counterpart in the oxidation of α-methylstyrene. SBA15-[Mn(TCPP-R*)Cl] catalyzed epoxidation of styrene was achieved within 8 h and optically active styrene oxide was obtained in 89% ee and 90% yield. Likewise, styrene derivatives (*trans*-β-methylstyrene, indene), conjugated *cis*- and *trans*-disubstituted olefins (e.g. *cis*- and *tans*-stilbene) and terminal olefins were converted effectively to their corresponding epoxides in 63–99% ee under the Mn(III)-catalyzed conditions. The catalyst could be recycled five times without any significant loss in activity.

1. Introduction

Epoxides are highly interesting synthons in organic chemistry due to their high reactivity. This is especially true for single enantiomers as a basis to introduce chirality in an early stage in the multistep synthesis of a complex final product. One example of such a synthon is (1S,2R)-indene oxide. (1S,2R)-indene oxide is used for the preparation of *cis*-aminoindanol in a Ritter reaction [1]. *Cis*-aminoindanol is the main precursor in the synthesis of CRIXIVAN® [2] which is the world's most widely used protease inhibitor for the treatment of AIDS [3]. A lot of chemical compounds used in pharmaceutical formulations feature one or more chiral centers. Each enantiomer of these chiral compounds exhibits different biological activities in living systems during biomedical and pharmacological processes. One enantiomer sometimes shows high toxicity while another is effective [4].

Oxidation of hydrocarbons with molecular oxygen is catalyzed by cytochrome P-450 enzymes [5]. The protein unit of natural hemoproteins manages to achieve the active site. For mimicking the natural enzyme, designing the skeleton of the model so that to select the access of the substrate to the metal center is a crucial object [6] Over the last decades, metalloporphyrins have been successfully used as models for the cytochrome P-450 enzymes, with respect to the oxidation of organic compounds such as hydrocarbons. Porphyrin and metalloporphyrin molecules have unique chemical, physical, electronic structures and properties and play a number of important roles in molecular binding, reaction catalysis, energy and electron transfer, and light absorption [7–10]. Current interest in this area is directed toward developing oxidation catalysts that combine the versatility of homogeneous metalloporphyrins with the advantages of heterogeneous systems. Supported metalloporphyrins matrice present advantages such as prevention of catalyst intermolecular self-oxidation and easy recovery and reuse of the catalyst. To this end, metalloporphyrins have been chemically and physically anchored on a wide variety of solid supports and the chemistry of the resulting materials compared with those of homogeneous counterparts. Furthermore, it is possible to provide a medium similar to the protein chain in natural hemoproteins by choosing an appropriate support for the metalloporphyrin.

Chiral porphyrins are effective catalyst for olefin epoxidation [6]. In comparison to much studied Mn(salen) derivatives, chiral porphyrin catalysts give better ee values in the epoxidation of terminal olefins and generally afford higher turnover numbers and frequencies. The incorporation of a chiral porphyrin into SBA-15 channels and its chiral recognition has been studied [11]. It has been also reported that the D-alanine interaction with the mesoporous composite SBA-15 is stronger than its optical antipode.

* Corresponding author.
E-mail address: monfared@znu.ac.ir (H. Hosseini Monfared).

http://dx.doi.org/10.1016/j.jcat.2017.05.014
0021-9517/

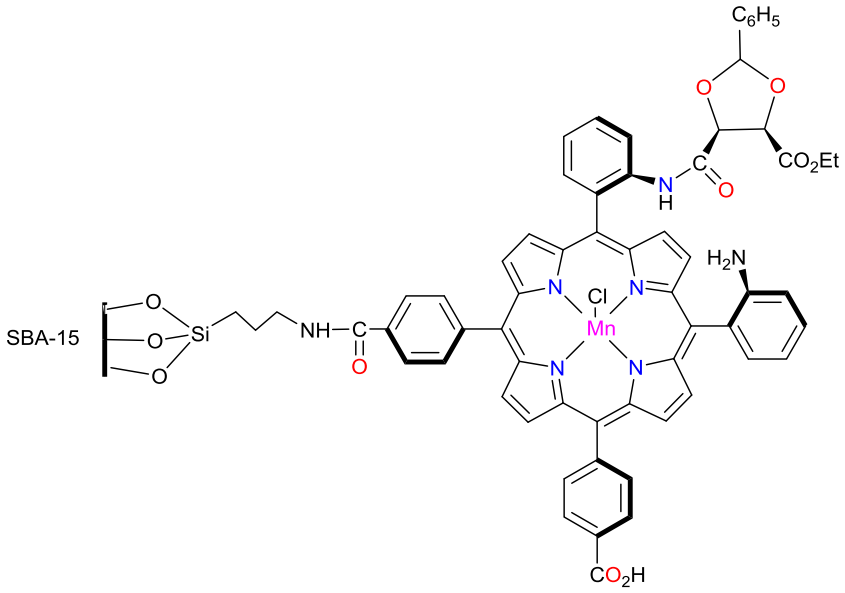

Fig. 1. Catalyst SBA15-[Mn(TCPP-R*)Cl].

Mesoporous SBA-15 silica has a regular hexagonal array of uniform channels with diameters 4.6–30 nm, high internal surface area of about 700–1000 $m^2 g^{-1}$, high thermal and hydrothermal stabilities and large pore volume [12–14]. The large specific surface area and pore volume can enhance the loading amounts of the metal catalyst and increase its catalytic efficiency, while well-defined pore arrangement can avoid the aggregation of catalytic active species and maintains excellent stereocontrol performance. The confinement effect of the nanopores of SBA-15 can provide a medium similar to the protein chain in natural hemoproteins. Because of these characteristics, SBA-15 provides a suitable support for catalysts for heterogenization [15–17]. However, there still exist some problems for the SBA-15 supported catalysts. The active species are easily leaching into the reaction medium as the weak interaction between the active species and SBA-15.

In spite of numerous reported chiral porphyrin structures, a few are efficient for enantioselective epoxidation catalysis [6]. Mixed condensation of 2,6-dinitro-4-tert-butylbenzaldehyde, pentafluorobenzaldehyde and pyrrole gave a mixture of soluble di-, tetra- and hexa-nitroporphyrins that afforded di-, tetra- and picket porphyrins [18]. However, epoxidation of styrene using iron complex of this porphyrin in the presence of PhIO afforded styrene oxide with very low ee values. It seems that providing more access to the catalytic active site will increase the enantioselectivity and facilitates the approach of the olefin. On the other hand, it has been proved that the presence of bulky chiral auxiliaries on Fe- and Mn-porphyrin complexes shows high regio- and enantioselectivities in the epoxidation of olefins. Additionally, the presence of electron-withdrawing groups or imposing nonplanar distortion on metalloporphyrin increases its activity. Meso-para-carboxy and meso-ortho-nitrophenyl substituted chiral porphyrins are appropriate candidates that can provide more access to the catalytic active site, facilitate the approach of the olefin and increase the enantioselectivity. They can be immobilized on cationic functionalized silicas by electrostatic interaction. Silica with amino functional group can also be used for heterogenization of metalloporphyrins. In the oxidation reactions, both steric hindrance and electron withdrawing properties of ortho-nitro groups improve the stability of metalloporphyrin catalysts. The nitro group can also be used as linker to attach porphyrins to other materials [19].

Effective catalytic reactions are developing every day due to competitive efforts of the researchers in industry and academia. While the field is progressing rapidly, many significant challenges remain in asymmetric catalysis [20]. Developing highly active catalysts that feature broad substrate scopes that can function under mild and simple reaction conditions remain key problems. It is especially important to identify effective catalysts that are based on readily available starting materials and reagents. Herein we report on a highly efficient chiral catalyst derived from a chiral Mn(III) porphyrin by an easy to synthesis and immobilized onto mesoporous silicate SBA-15 (Fig. 1). The catalyst activity was evaluated in the oxidation of vinyl aromatic compounds, such as indene, styrene and its derivatives by molecular dioxygen. In addition to site isolation and heterogenization of the catalyst, mesoporous support SBA-15 improved the enantioselectivity of the homogeneous catalyst.

2. Experimental section

2.1. Materials and equipments

All chemicals of highest grade were prepared from commercial sources and used as received. Mesoporous SBA-15 and aminofunctionalized SBA-15 material, SBA15-NH_2 were synthesized according to the procedure described already [21,22]. Diethyl-2,3-O-benzylidene-L-tartrate was prepared following a similar procedure reported in the literature [23].

The reaction products of the oxidation were determined and analyzed by HP Agilent 6890 gas chromatograph equipped with an HP-5 capillary column (phenyl methyl siloxane 30 m × 320 μm × 0.25 μm) with flame-ionization detector. The enantiomeric excess (ee%) was determined by chiral GC (HP 6890-GC) using a SGE-CYDEX-B capillary column (25 m × 0.22 mm × 0.25 μm). ^1H NMR spectra of the reaction mixture (without purification) were recorded on a Bruker 250 MHz spectrometer. UV–Vis spectra of solutions were recorded on a Shimadzu 160 spectrometer. Fourier transform infrared (FT-IR) spectra were run using a Perkin-Elmer 597 spectrophotometer after making pellets with KBr powder. Powder X-ray diffraction patterns were collected at the Bruker, D8ADVANCE, Germany, wavelength 1.5406 Å (Cu Kα), voltage: 40 kV, current, 40 mA. The size and morphology of the solid compounds were recorded using a Hitachi F4160 scanning electron microscope (SEM) operated at an acceler-

ating voltage of 10 kV and the textural properties determined from N_2 adsorption isotherms measured on a Belsorp mini II (Japan) instrument.

2.2. Synthesis of 5,10(or 15)-bis(4-carboxyphenyl)-15(or 10),20-bis(2-nitrophenyl)porphyrin, H_2TCPP-NO_2

5,10-bis(4-carboxyphenyl)-15,20-bis(2-nitrophenyl)porphyrin was synthesized according to the literature [19]. Nitrobenzene (4.28 ml) and pyrrole (0.14 ml, 2.02 mmol) were added to the solution of 2-nitrobenzaldehyde (0.10 g, 0.66 mmol) and 4-carboxybenzaldehyde (0.20 g, 1.36 mmol) in propionic acid (10 ml). The reaction vessel was shielded from ambient light and the mixture was heated at 120 °C for 1 h. The solvent was removed and the solid porphyrin purified by column chromatography on silica with dichloromethane/acetone/acetic acid (8:2:0.1) as eluent. The product was a purple colored solid. Yield 6% (0.03 g). UV–Vis in DMF: λ_{max} (log ε, $dm^3\,mol^{-1}\,cm^{-1}$): 420 (5.34), 515 (4.72), 550 (4.61), 590 (4.51) and 645 (4.37). FT-IR (KBr, cm^{-1}): 3433 (s, br, O—H), 1695 (vs C=O), 1405 (m, C—O), 1244 (s, C—O), 1522 (s, NO_2), 1346 (s, NO_2), and 1606 (m, C=C). The high frequency region of the ^{1}H NMR spectra shows the chemical shifts for pyrrole hydrogens (beta-H). ^{1}H NMR (250 MHz, DMSO): $\delta = -3.00$ (s, 2H, N—H), 7.60–8.00 (m, 6H, Hβ-nitro), and 8.10–8.84 (m, 16H, aryl; m, 2H, Hβ-carboxy). Anal. Calcd for $C_{46}H_{28}N_6O_8$: C, 69.69; H, 3.56; N, 10.60. Found: C, 70.33; H, 4.06; N, 10.89.

2.3. Synthesis of 5,10-bis(2-aminophenyl)-15,20-bis(4-carboxyphenyl)porphyrin, H_2TCPP-NH_2

Reduction of the nitro groups of the porphyrin was performed following a reported procedure with modifications [24]. The synthesized H_2TCPP-NO_2 (0.10 g, 0.13 mmol) was dissolved in concentrated hydrochloride acid under nitrogen. After addition of tin(II) chloride dihydrate (0.28 g, 1.26 mmol) the resulting green mixture was stirred for 45 min at room temperature and then heated at 65 °C for 30 min. Then the mixture was cooled in ice to 0 °C, concentrated aqueous NH_3 solution was added slowly to bring pH of the mixture to 10. The product was extracted by addition of $CHCl_3$ (40 mL) and stirring vigorously for 1 h; the procedure was repeated twice. The organic fractions were combined, washed with water and followed by filtration to obtain a dark purple solid. Yield 42% (0.04 g). UV–Vis in DMF: λ_{max} (log ε, $dm^3\,mol^{-1}\,cm^{-1}$): 425 (3.94), 515 (3.40), 550 (3.29), 590 (3.18) and 645/650 (3.04). FT-IR (KBr, cm^{-1}): 3422 (s, br, O—H), 3126 (N—H), 1730 (vs C=O), 1607 (m, C=C), 1387 (m, C—O), and 1269 (m, C—O). Anal. Calcd for $C_{46}H_{32}N_6O_4$: C, 75.40; H, 4.40; N, 11.47. Found C, 77.00; H, 2.80; N, 10.55.

2.4. Synthesis of chiral porphyrin, H_2TCPP-R*

The solution of diethyl-2,3-O-benzylidene-L-tartrate (0.012 g, 0.041 mmol) and 5,10-bis(2-aminoophenyl)-15,20-bis(4-carboxy phenyl) porphyrin (0.01 g, 0.014 mmol) in methanol was refluxed for 2 h and resulting product was washed with water and dried in air [25]. A dark purple colored oily product was obtained. Yield 15% (0.19 g). FT-IR (KBr, cm^{-1}): 3426 (s, br, O—H), 2961 (w), 2780 (w), 1707 (shoulder, C=O), 1627 (m, C=C), 1405 (w, C—O), and 1261 (m, C—O).

2.5. Synthesis of [Mn^{III}(TCPP-R*)Cl]

Metalation of the porphyrin was performed by the method of Alder under nitrogen [19]. The mixture of free base porphyrin H_2-TCPP-R* (0.20 mmol) and 10 equivalents manganese(II) chloride tetrahydrate (2.0 mmol) in DMF (15 mL) was refluxed for 7 h. The manganese porphyrin was precipitated from the reaction medium by adding HCl (15 mL, 0.10 mol dm^{-3}) and cooling the reaction flask in an ice bath. The precipitate was recovered by centrifugation and the supernatant, which contained DMF and excess manganese(II) salt, was discarded. The target product, a dark purple-colored solid, was obtained by washing with HCl (30 mL, 0.10 mol dm^{-3}) and purifying by silica column chromatography. Yield 76% (0.005 g). FT-IR (KBr, cm^{-1}): 3427 (s, br, O—H), 2922 (w), 2852 (w),1731 (s, C=O), and 1655 (m, N—C=O). UV–Vis in DMF: λ_{max} (log ε, $dm^3\,mol^{-1}\,cm^{-1}$): 467 (2.96), 560 (2.30) and 605 (2.09).

2.6. Organofunctionalization of SBA-15 (SBA15-NH_2)

Mesoporous SBA-15 was synthesized according to the procedure described in the literature [21]. The SBA-15 was activated under vacuum at 150 °C for 3 h [22]. The mixture of SBA-15 and 3-aminopropyl triethoxysilane (2.17 g, 9 mmol per 3 g of SBA-15) in 100 cm^3 of dry toluene was refluxed under nitrogen for 6 h. Then Soxhlet extraction with dichloromethane (for 12 h) yielded the white color NH_2-functionalized SBA-15 material (SBA15-NH_2). IR (KBr, cm^{-1}): 3441 (m, O—H), 1077 (vs Si—O), 810 (s), and 466 (s). Anal. found for SBA15-NH_2: C, 7.73; H, 1.90; N, 3.56.

2.7. Synthesis of SBA15-[Mn^{III}(TCPP-R*)Cl]

Covalent binding of the chiral Mn-porphyrin to SBA15-NH_2 was carried out according to a modified reported procedure [26]. In a round bottom flask, the amino functionalized SBA-15 (0.31 g) and dicyclohexylcarbodiimide (DCHC) (0.02 g) were suspended in 10 mL of N,N-dimethylformamide (DMF). The solution of [Mn^{III}(TCPP-R*)OAc] (0.10 g) in DMF (5 mL) was added dropwise to the suspension and the mixture was refluxed at 140 °C for 8 h. The resulting solid was isolated and exhaustively washed sequentially in a Soxhlet extractor with DMF, CH_2Cl_2 and methanol for removing the porphyrin bonded by electrostatic interactions to SBA15-NH_2. A brown colored solid product was obtained. Yield 0.405 g. Anal. found for SBA15-[Mn^{III}(TCPP-R*)Cl]: C, 16.93; H, 2.21, N, 3.65; Mn, 0.35%.

2.8. Catalytic aerobic oxidation of hydrocarbons

The oxidation of hydrocarbons was performed in a 25-mL round-bottom flask equipped with a condenser in a thermostated oil bath at 45 °C. In a typical experiment the flask was charged with the suspension of catalyst SBA15-[Mn^{III}(TCPP-R*)Cl] (10.0 mg; contains 63.7 μmol Mn), 5 mL acetonitrile, 0.10 g chlorobenzene as internal standard, substrate and 5 mmol isobutyraldehyde. Dioxygen was provided using an oxygen balloon. The reaction mixture was stirred at 45 °C for 8 h. At appropriate intervals, aliquots were removed and analyzed by GC-FID. The products were identified with authentic samples and ^{1}H-NMR spectroscopy.

3. Results and discussion

3.1. Synthesis of catalyst

The chiral porphyrin H_2TCPP-R* and immobilized [Mn(TCPP-R*)Cl] on mesoporous SBA-15 were prepared according to Scheme 1. 5,10(or 15)-bis(4-carboxyphenyl)15(or 10),20-bis(2-nitrophenyl) porphyrin (*cis*- or *trans*-isomer) (H_2TCPP-NO_2) was prepared according to the method of Assis [19]. Analysis of the ^{1}H- and ^{13}C-NMR spectra (Figs. S1 and S2 in the ESI) suggests the presence of the *cis* and *trans* isomers which are not possible to separate them under the conditions used. According to the synthesis route

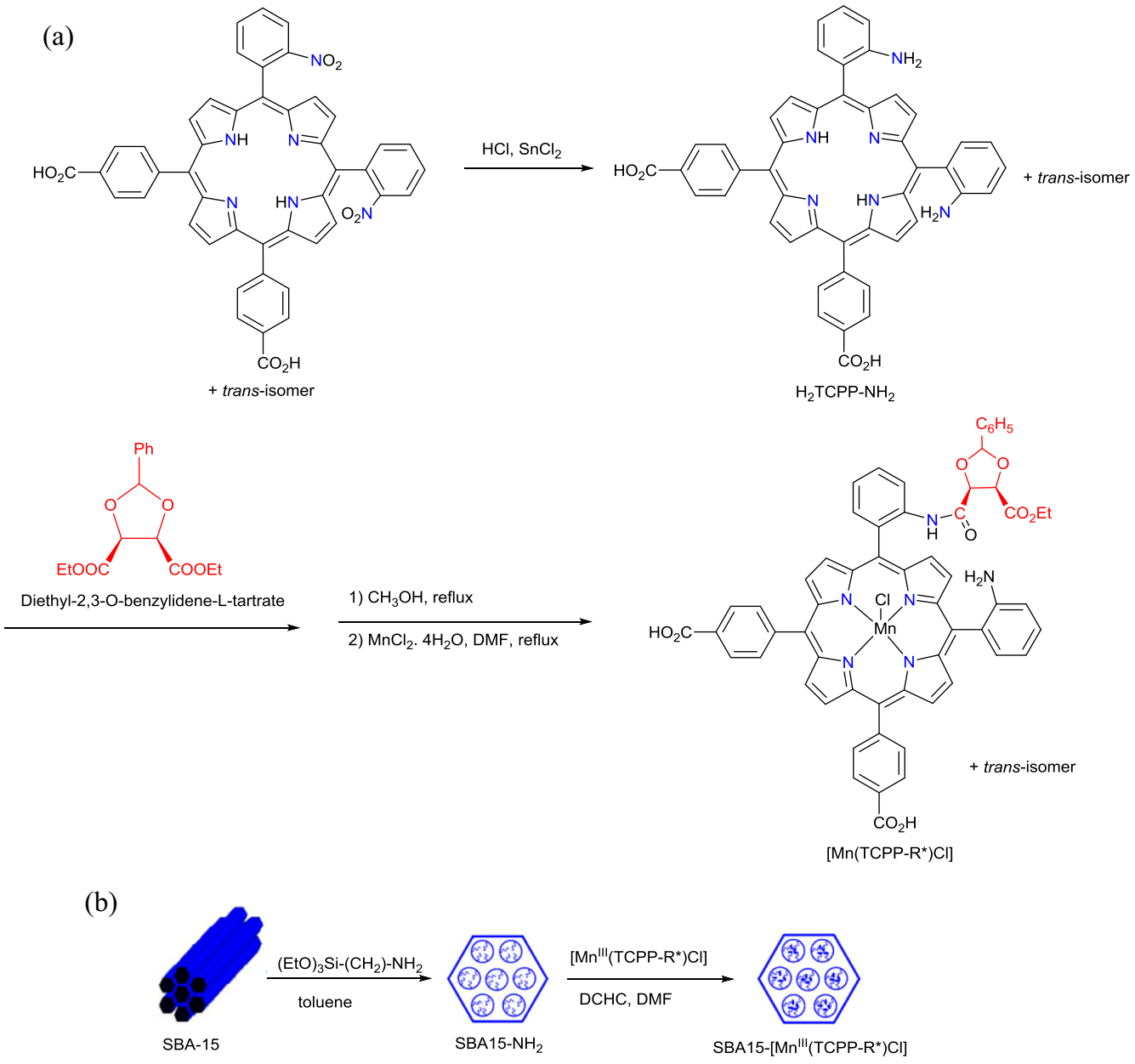

Scheme 1. The synthesis route for (a) the chiral Mn-porphyrin and (b) SBA15-[Mn^{III}(TCPP-R*)Cl]; (DCHC = dicyclohexylcarbodiimide; DMF = N,N'-dimethylformamide).

(Scheme 1), first the nitro groups of H_2TCPP-NO_2 were reduced to get H_2TCPP-NH_2. The treatment of H_2TCPP-NH_2 with diethyl-2,3-benzylidene-L-tartrate (-R*) produced H_2TCPP-R* which was then metallated to obtain [Mn^{III}(TCPP-R*)Cl]. The corresponding ^{1}H- and ^{13}C-NMR spectral data confirmed the synthesis of intermediates and H_2TCPP-R* (Figs. S3–S6). The Mn(II) is oxidized to Mn (III) by air during the reaction. Complex [Mn^{III}(TCPP-R*)Cl] covalently bonded to SBA15-NH_2 in DMF in the presence of DCHC. The porphyrin H_2TCPP-R* contains chiral ethyl-2,3-O-benzylidene-L-tartrate moiety. We hypothesized that a chiral substituent on the phenyl groups should be able to induce a preference for one of the two enantiomorphic conformations. [Mn(TCPP-R*)Cl] and mesoporous silica SBA-15 were to resemble the active center and skeleton of the enzyme, respectively. The catalysis activity studies of the sample showed that the Mn^{III}(TCPP-R*)Cl] complex grafted in SBA-15 channels have high asymmetric epoxidation activity with better enantioselectivity.

3.2. Analysis of the catalyst

The synthesis of Mn-porphyrin was confirmed by the FT-IR spectra analyses. In the FT-IR spectrum of H_2TCPP-NO_2, the strong absorption bands of the NO_2 group from asymmetric and symmetric deformations appear at 1524 cm^{-1} and 1349 cm^{-1}, respectively (Fig. 2). Reduction in the nitro group was clearly demonstrated by the disappearance of the NO_2 absorptions in H_2TCPP-NH_2 (Fig. 2 and Fig. S7 in the ESI). The absorption band around 1695 cm^{-1} is assigned to the stretching vibration of carboxylic acid CO_2.

Metalation of the porphyrin ligand proved by comparison of the FT-IR spectra of H_2TCPP-R* and [Mn(TCPP-R*)Cl] (Figs. S8 and S9 in the ESI). In the FT-IR spectra of SBA-15 and SBA15-[Mn(TCPP-R*)Cl] the absorptions at 3424 cm^{-1} and 1634 cm^{-1} can be attributed to the O—H stretching vibration and δ(O—H) modes arising from the adsorbed water (Fig. 3). The characteristic antisymmetric ν_{as}(-Si—O—Si) vibration bands of the [SiO_4] units are observed at

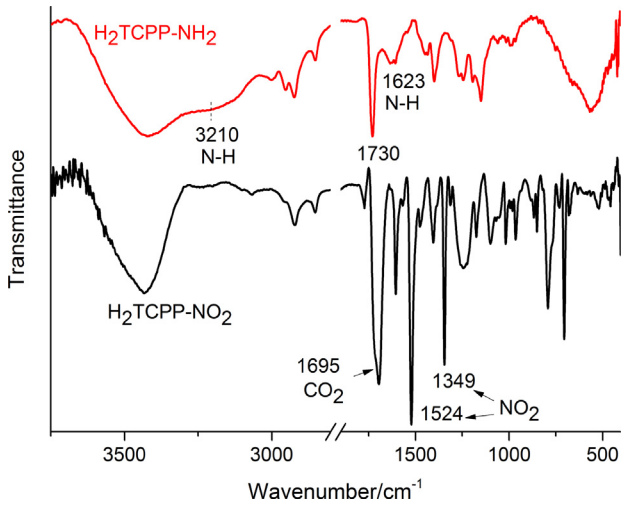

Fig. 2. An overlay of the FT-IR spectra of H_2TCPP-NO_2 and H_2TCPP-NH_2.

1209 (shoulder) and 1081 cm^{-1}. The band at 803 cm^{-1} is assignable to ν_s(Si—O—Si) modes. The small shoulder band at 962 cm^{-1} is assignable to (Si—OH). The bending vibration band of O—Si—O unit observed at 464 cm^{-1}. Interestingly, the IR band located at 3424 cm^{-1} due to the surface OH group appeared to decrease in intensity after the functionalization reaction, and thus confirming that 3-aminopropyltriethoxysilane was trapped inside SBA-15 pores through the reaction of surface silanols with functional groups [27]. In the spectrum of SBA15-NH_2, the broad peak at 3300 cm^{-1} is due to the NH_2 stretching vibration [28]. The N—H bending appeared at 1727 cm^{-1}; its intensity decreased in SBA15-[Mn(TCPP-R*)Cl]. In addition, two new IR bands at 2960 and 2850 cm^{-1} corresponding to the CH_2 asymmetric and symmetric stretching vibrations in the propyl chain of silylating reagents, respectively. The band at 1453 cm^{-1} is probably due to CH_2 scissor bending vibration [29]. Additionally, the peak at about 3424 cm^{-1} broadened after incorporation the porphyrin into SBA-15. These results indicate the successful incorporation of the porphyrin into the SBA-15 channels, which is well agreement with above measurement results [30]. The possibility that grafting of [Mn(TCPP-R*)Cl] onto SBA-15 to take place through the CO_2H group which is *trans* to the R* (Fig. 1) cannot be excluded. However, involvement of the both —CO_2H groups in grafting is less probable because of the steric hindrance. The very broad band about 3424 cm^{-1} for SBA15-[Mn(TCPP-R*)Cl] (Fig. 3c) confirms the involvement of one of the CO_2H groups.

UV–Vis absorption spectra of H_2TCPP-NO_2, H_2TCPP-NH_2 and H_2-TCPP-R* in DMF showed a typical Soret band at 420 nm and four Q bands in the visible region (Fig. 4). By metalation of H_2TCPP-R* the Soret band shifted to 467 nm and two Q bands appeared at 560 and 605 nm. The observed bands confirmed the metalation process [31]. The observation of flattened in the spectra of Fig. 4b–d shows that there are some kind of aggregation.

UV–Vis spectroscopy shows the porphyrin aggregation, where the Soret band undergoes either a bathochromic (J-type) or a hypsochromic (H-type) aggregation shift compared to the porphyrin monomers. The Soret band of face-to-face dimers and the higher H-type aggregates are seen at shorter wavelengths with respect to porphyrin monomer, while for that of the higher edge-to-edge J-type aggregates appear at higher wavelengths [32]. The higher self-aggregates without a J-type arrangement exhibited a broad band near the wavelength region of the monomer Soret band [33]. Therefore, reduction in the intensity of H_2TCPP-R* Soret band with respect to that of H_2TCPP-NH_2 confirms the higher aggregation of H_2TCPP-R* monomers through hydrogen bonding and/or π-π interactions. Likewise, reduction in the intensity and a bathochromic shift of the Soret band of H_2TCPP-NH_2 show somewhat its aggregation by reduction of the NO_2 groups. The monomers of [Mn(TCPP-R*)Cl] indicate the highest aggregation. In addition, the Soret band of [Mn(TCPP-R*)Cl] is splitted by the coordination of solvent (DMF) as it happens when there is more than one axial ligand.

Thermogravimetric analysis (TGA) of SBA15-[Mn(TCPP-R*)Cl] was performed to analyze the thermal stability of the sample and to verify the amount of organic composite in the sample. The TGA curve showed an initial weight loss due to solvent liberation and a high thermal stability up to 145 °C. It showed weight loss in the range from 145 °C to 434 °C (weight loss ≈ 10%) and 434 °C to 634 °C (≈10%) due to the decomposition of benzylidene-L-tartrate substituent (Figs. S10 and S11 in the ESI). The porphyrin ring is stable up to 634 °C [34]. The weight loss analysis showed that the total loss of the sample was about 27%.

The small-angle XRD patterns of SBA-15, SBA15-NH_2, and SBA15-[Mn(TCPP-R*)Cl] showed two well-resolved diffraction peaks with a very intense peak at 2θ of 0.9–1.18° for (100) and one peak at 2θ of 1.4–1.8° for (200), Fig. 5. The patterns are typical for the highly ordered SBA-15 mesoporous structure. The strong (100) peak of SBA15-[Mn(TCPP-R*)Cl] shows the stability of the mesoporous SBA-15 framework when the chiral Mn-porphyrin grafted on it. The intensity of the peak at 2θ of 1.4–1.8° for

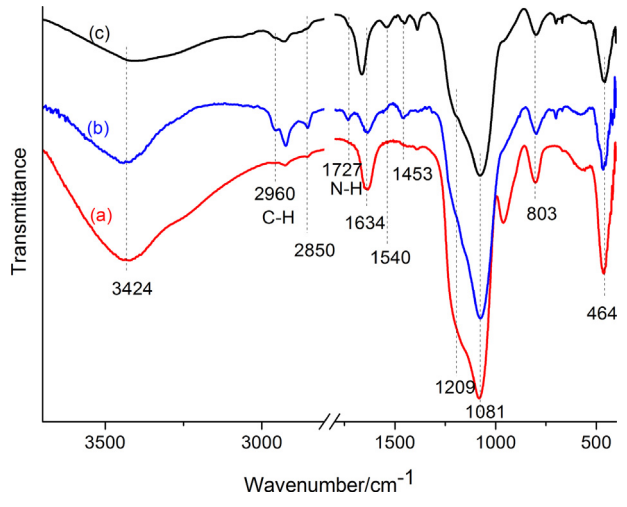

Fig. 3. FT-IR spectra of (a) SBA-15, (b) SBA15-NH_2 and (c) SBA15-[Mn(TCPP-R*)Cl].

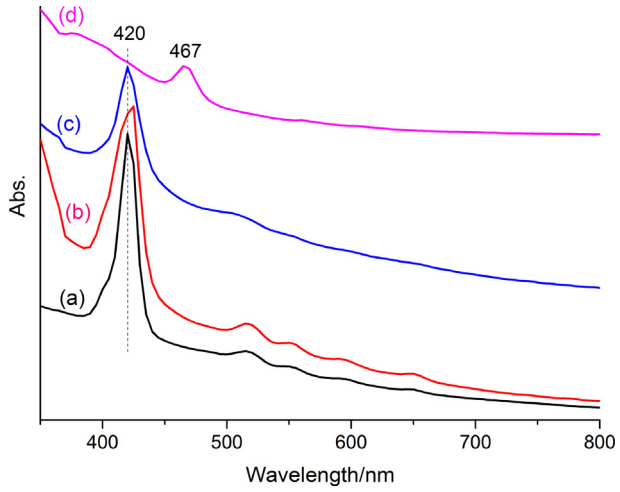

Fig. 4. UV–Vis spectra of (a) H_2TCPP-NO_2, (b) H_2TCPP-NH_2, (c) H_2TCPP-R* and (d) [Mn(TCPP-R*)Cl] in DMF.

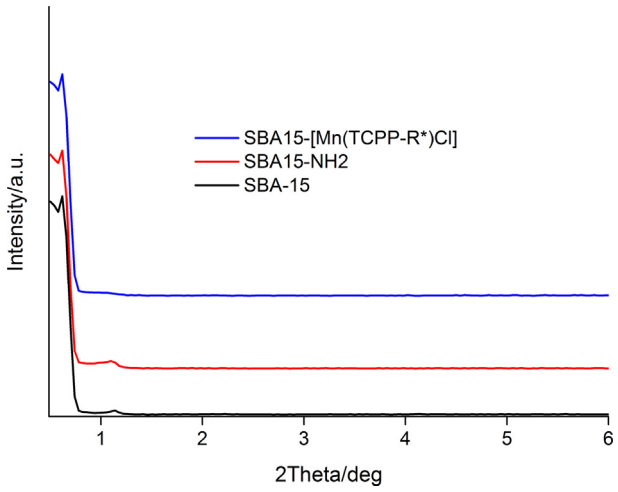

Fig. 5. The small angle X-ray powder diffraction (SXRD) patterns of unmodified SBA-15, SBA15-NH_2 and SBA15-[Mn(TCPP-R*)Cl].

SBA15-[Mn(TCPP-R*)Cl] is slightly lower than that measured for SBA-15. This evidence confirms that the immobilization of the Mn-porphyrin primarily occurred inside the mesoporous channels, probably caused by the pore filling effect of the SBA-15 channels or by the anchoring ligands on the surface of SBA-15 [35].

SEM analyses revealed curved cylindrical particles of SBA-15 that remained unaffected on immobilization of the Mn-porphyrin thus confirming the retention of the physical structure of the siliceous material (Fig. 6). The curved cylinder-particles have a diameter of about 500–700 nm and length up to 1–2 μm, which is typical morphology for SBA-15 mesoporous materials. Furthermore, the SBA15-[Mn(TCPP-R*)Cl] is stable and preserved its morphology at the end of the catalytic oxidation reaction (Fig. 6c).

N_2 adsorption–desorption isotherms of SBA-15, SBA15-NH_2 and SBA15-[Mn(TCPP-R*)Cl] show type IV isotherms (Fig. 7), characteristic of the mesoporous materials (2–50 nm) with completely reversible nature, uniformly sized mesoporous. It is well known that the introduction of homogenous catalysts on porous supports shows a decrease in its specific surface area and pore volume [36]. The BET surface area, pore diameter and pore volume of calcined SBA-15, SBA15-NH_2 and immobilized complex [Mn^{III}(TCPP-R*)Cl] are given in Table 1 suggesting that the complex [Mn^{III}(TCPP-R*)Cl] is present inside the pores of the support material. The catalyst support, mesoporous calcined SBA-15, shows a high surface area of 2643 m^2/g and pore volume of 1.00 cm^3/g. After functionalization, the surface area gets reduced to 793 m^2/g and pore volume 0.53 cm^3/g for SBA15-[Mn(TCPP-R*)Cl] samples. The reduction in the surface area and pore volume is due to the lining of the walls of SBA-15 with the organic moieties. The N_2-adsorption measurement studies also confirm the presence of manganese complex inside the channels of SBA-15.

3.3. Catalysis of olefin oxidation

The supported chiral Mn-porphyrin was used in the aerobic oxidation of α-methyl styrene as representative olefin. Preliminary experiment findings disclosed a significant influence of isobutyraldehyde and solvent on the activation of oxygen for the oxidation reaction. Of the examined solvents (acetonitrile, methanol, ethyl acetate and *n*-hexane), acetonitrile afforded a favored medium for the oxidation and resulted in 100% conversion and enantiomeric excess (ee) 81% in 8 h. The catalyst support SBA-15 did not catalyze the reaction under our optimum condition (at 45 °C in CH_3CN). Co-oxidation of α-methyl styrene and isobutyraldehyde under the investigated conditions led to the formation of α-methyl styrene oxide (85%), benzaldehyde (15%) and isobutyric acid (Fig. 8). Fig. 8 depicts the time courses for the enantioselective α-methyl styrene and 1-decene oxidation using SBA15-[Mn(TCPP-R*)Cl] as catalyst. The oxidation of α-methyl styrene proceeded monotonically up to completion. However, the oxidation of 1-decene stopped after 6 h (conversion 76%) in spite of its higher oxidation rate with respect to α-methylstyrene (Fig. 8).

The composite SBA15-[Mn(TCPP-R*)Cl] showed high activity in the oxidation of styrene and *trans*-β-methylstyrene by/O_2/^{i}PrCHO in CH_3CN at 45 °C (Table 2, entry 2 and 3). Epoxide selectivity (90%) and ee (89%) obtained in the oxidation of styrene (entry 3) were higher than those of α- and β-methylstyrene. The steric

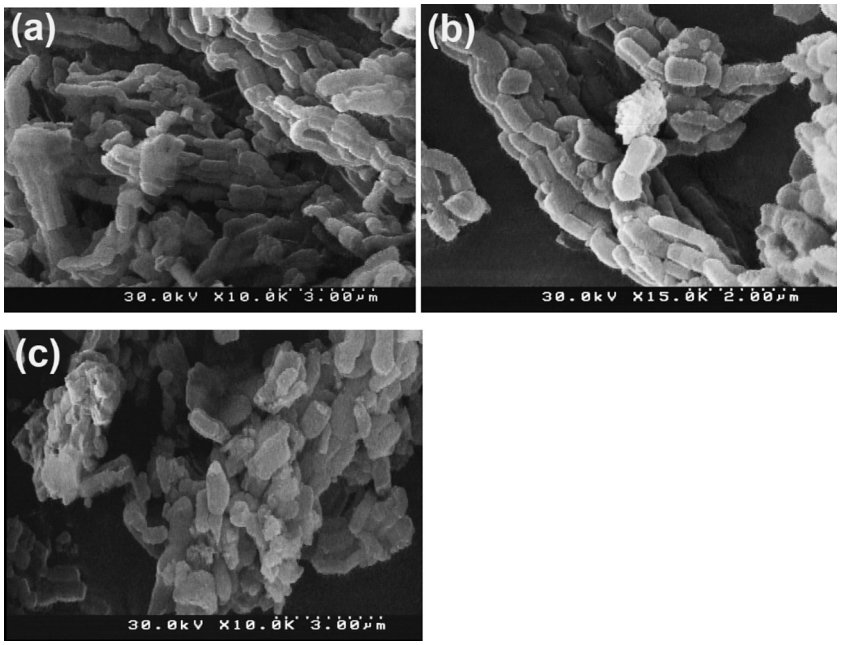

Fig. 6. SEM images of (a) SBA-15, (b) SBA15-[Mn(TCPP-R*)Cl] and (c) recovered SBA15-[Mn(TCPP-R*)Cl].

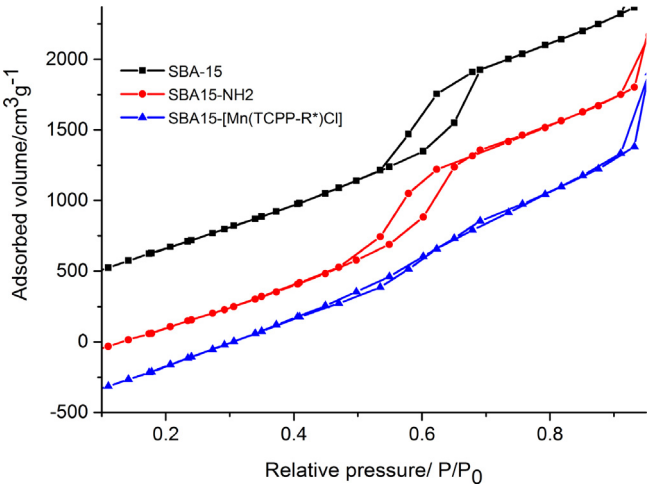

Fig. 7. Nitrogen adsorption–desorption isotherms and volume plots of SBA-15, SBA15-NH_2 and SBA15-[Mn(TCPP-R*)Cl].

Table 1
Surface characteristics of the synthesized SBA-15, aminopropyl funtionalized SBA-15 and immobilized [Mn(TCPP-R*)Cl].

Compound	Surface area (m^2/g)	Pore diameter (nm)	Pore volume (cm^3/g)
SBA-15	2643	2.38	1.00
SBA15-NH_2	497	2.38	0.90
SBA15-[Mn(TCPP-R*)Cl]	793	2.34	0.53

effects of the olefin substituents on enantioselectivity are also evidently seen in the oxidation of *cis*- (63% ee) and *trans*-stilbene (74% ee) and 1-phenylcyclohexene. 1-Phenylcyclohexene with three substituent showed the lowest conversion 13% and ee 38% (entry 4).

One highly remarkable feature of catalyst SBA15-[Mn(TCPP-R*)Cl] is in oxidation of indene with > 99% ee and > 99% epoxide yield (entry 7). Optically active (1S,2R)-indene oxide is a useful intermediate for the synthesis of *cis*-aminoindanol [1] and an inhibitor for the treatment of AIDS [2,3]. (1S,2R)-Indene oxide (87% ee) is accessible by chemical epoxidation of indene with a Mn^{II}Salen complex as Jacobsen catalyst [37].

Although the highest ee (>99%) was observed for 1-decene and 1-octene (entries 8 and 9), the activity of 1-octene (conversion 90%) and 1-decene (79%) with flexible mono-substituents was lower than that of the other olefins.

In addition to the oxidation of aryl olefins, SBA15-[Mn(TCPP-R*)Cl] could catalyze aerobic oxidation of cyclohexene and *cis*-cyclooctene with >99% epoxide selectivity (not shown in Table 2). This observation excludes the involvement of hydroxyl and alkylperoxy radicals which tend to lead to allylic position oxidation of cyclohexene [38].

The rate of aerobic catalytic oxidation of olefins by homogeneous [Mn(TCPP-R*)Cl] (Table 3) was higher than its immobilized form under the same reaction conditions (at 45 °C in CH_3CN). It seems that there is the possibility of diffusion limitation, since active [Mn(TCPP-R*)Cl] species are in the one-dimensional channels of SBA-15 [39]. The mesoporous channels of the catalyst support SBA-15 (5–20 nm) have diffusion limitations for large feed molecules to enter into unidirectional channels of the SBA-15 [40,41] and gave as well higher selectivity to bulky product. These viewpoints confirmed that there could be some transport limitations in channels of SBA-15. However, the oxidation rate (conversion 100% in 8 h), epoxide selectivity and ee were the same for both homogeneous and heterogeneous catalysts in the oxidation of indene (cf. Tables 2 and 3). In addition, the enantioselectivity of SBA15-[Mn(TCPP-R*)Cl] (ee 81%) in the oxidation of α-methylstyrene was higher than that of the unsupported homogeneous catalyst (ee 70%). These examples clearly suggest that the confinement effect from the nanochannels can improve the activity and chiral induction for the asymmetric catalysis. This is a highly valuable effect of the mesoporous channels of the support (SBA-15). Involvement of the site isolation effect of the support on active species and prevention from aggregation of [Mn(TCPP)-R*)Cl] on the catalytic activity cannot be excluded.

It has been already reported that the catalyst support can affect the catalytic properties of the heterogeneous asymmetric epoxidation [42]. Chiral Mn(salen) catalysts immobilized in the nanopores of SBA with the optimized pore size exhibit higher chemical selectivity and enantioselectivity than those anchored on the external surface of supports for the asymmetric epoxidation [43]. The factors including the confinement effect, the stereo properties of the linkages of the heterogeneous chiral catalysts and for hydrophobic

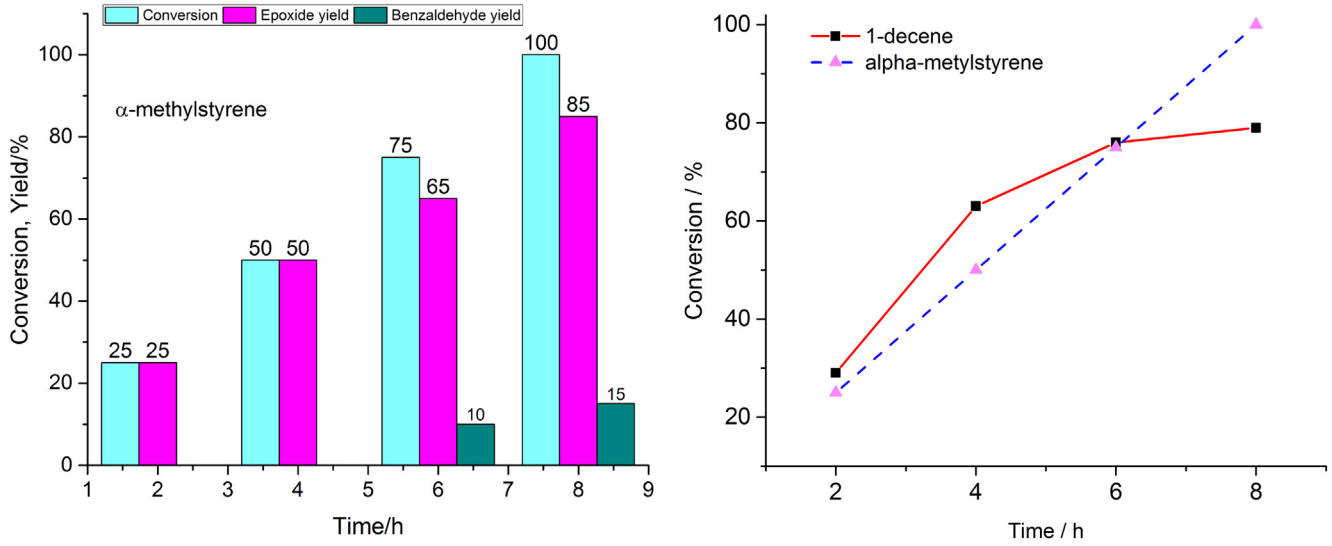

Fig. 8. Time courses for the Mn-porphyrin catalyzed α-methylstyrene oxidation (left) and comparison of the rate of oxidation of α-methylstyrene and 1-decene (right). Conditions: SBA15-[Mn(TCPP-R*)Cl] 10.0 mg (63.7 μmol Mn), substrate 2 mmol, isobutyraldehyde 5 mmol, chlorobenzene 0.10 g, acetonitrile 5 mL, 45 °C, O_2 1 bar.

Table 2
Aerobic asymmetric oxidation of olefins catalyzed by SBA15-[Mn(TCPP-R*)Cl].[a]

Entry	Substrate	Conv. (%)[b]	Product(s)/yield (%)[b] (configuration)	Epoxide select. (%)	ee (%) (conf.)[c]
1		100	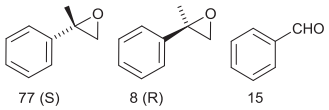 77 (S) 8 (R) 15	85	81 (S)
2	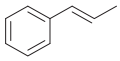	100	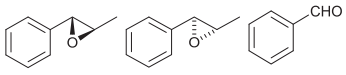 9 (R,R) 77 (S,S) 14	86	79 (S,S)
3		100	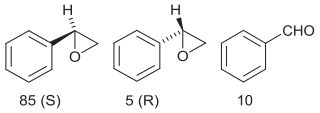 85 (S) 5 (R) 10	90	89 (S)
4		13	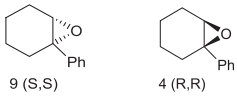 9 (S,S) 4 (R,R)	100	38 (S,S)
5		100	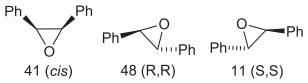 41 (*cis*) 48 (R,R) 11 (S,S)	100	63 (1R,2R)
6	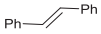	100	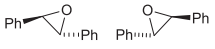 87 (R,R) 13 (S,S)	100	74 (1R,2R)
7		100	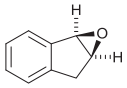	100	100 (R,S)
8		79	 79 (S)	100	99 (S)
9		90	 90 (S)	100	99 (S)

[a] Reaction conditions: SBA15-[Mn(TCPP-R*)Cl] 10.0 mg (0.0637 mmol Mn), substrate 2 mmol, isobutyraldehyde 5 mmol, solvent 5 mL, chlorobenzene 0.10 g, O_2 balloon, reaction temperature 45 °C, time 8 h.
[b] Conversions and yields calculated on the basis of the substrate.
[c] The enantiomeric excess (ee) values were determined by GC analysis on a chiral stationary phase (see Section 2).

Table 3
Aerobic asymmetric oxidation of olefins catalyzed by homogeneous [Mn(TCPP-R*)Cl].[a]

Entry	Substrate	Conv. (%)[b]/time (h)	Product(s)/yield (%)[b] (configuration)	Epoxide select. (%)	ee (%) (conf.)[c]
1	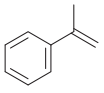	100 (3)	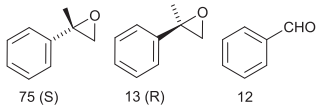 75 (S) 13 (R) 12	88	70 (S)
2	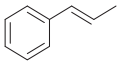	100 (2)	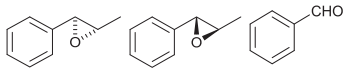 86 (S,S) 6 (R,R) 8	92	87 (S,S)
3	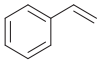	100 (2)	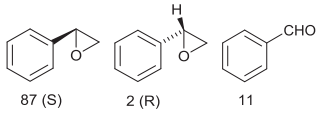 87 (S) 2 (R) 11	89	95 (S)
4		100 (8)	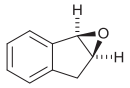	100	100 (R,S)
5		79 (6)	 79 (S)	100	99 (S)
6		95 (6)	 90 (S)	100	99 (S)

[a] Reaction conditions: [Mn(TCPP-R*)Cl] 1.00 mg, substrate 2 mmol, isobutyraldehyde 5 mmol, solvent 5 mL, chlorobenzene 0.10 g, O_2 balloon, reaction temperature 45 °C.
[b] Conversions and yields calculated on the basis of the substrate.
[c] The enantiomeric excess (ee) values were determined by GC analysis on a chiral stationary phase (see Section 2). Reported results are the average of two experiments.

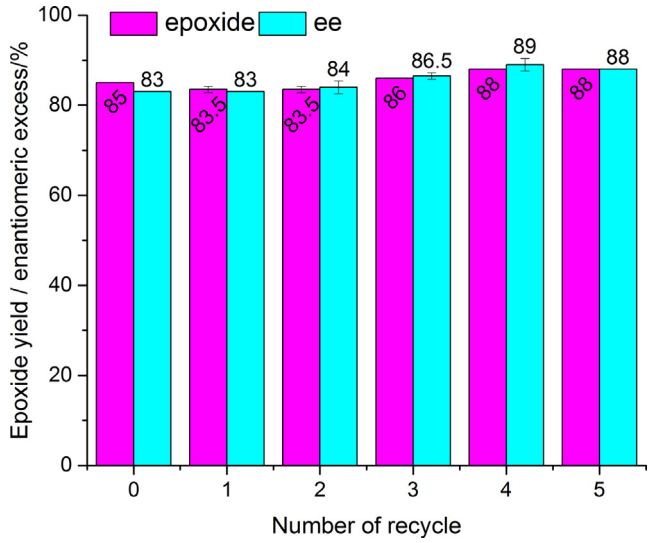

Fig. 9. Recycling experiments. Reaction conditions: SBA15-[Mn(TCPP-R*)Cl] 10.0 mg (63.7 μmol), α-methyl styrene (2 mmol), CH_3CN 5 mL, $^{i}PrCHO$ 5 mmol at 45 °C for 8 h. Total turnover number (total number of moles product/mole catalyst) = 157. Results are the average of two runs.

substrates the hydrophobic microenvironment in nanopores which affect the activity and enantioselectivity of asymmetric catalysis in nanopores.

3.4. Catalyst recycling

The recyclability of SBA15-[Mn(TCPP-R*)Cl] was examined using the oxidation of α-methyl styrene. The particles were separated at the end of the reaction by centrifugation, washed and reused five times. They showed outstanding reusability without significant catalytic activity losses (Fig. 9), and the morphology of particles retained after multiple oxidations (Fig. 6c). The FT-IR spectrum of the used and recovered SBA15-[Mn(TCPP-R*)Cl] after first and fifth times is the same as that of the fresh one (Fig. S12 in the ESI). More importantly, the epoxide yield and enantioselectivity increased gradually after each recycle. Total turnover number after five run was 157.

There was no Mn ion and no Mn–porphyrin leaching up to five cycles. Leaching of the Mn(III)-complex and/or Mn ion from the SBA-15 support was tested by filtration method. Accordingly, in a typical catalytic oxidation of α-methyl styrene, after 8 h the solid catalyst was separated by centrifugation. The screening of the resulting solution by atomic absorption method showed no detectable (<0.02 ppm) manganese. This confirmed that no leaching of the active supported Mn(III)-components occurred. The filtrate was also examined by UV–Vis spectrophotometer for the presence of the porphyrin and/or the Mn-porphyrin after each recycling experiment (Fig. S13 in the ESI). No detectable trace of H_2TCPP-R* or [Mn(TCPP-R*)Cl] was observed in the range 400–800 nm (compare with Fig. 4) which confirmed the absence of the porphyrin derivatives in the filtrate. Overall, the control experiments provided evidence that the observed catalytic results are derived by the heterogeneous catalyst and no leaching of the active component or demetalation occurs during the catalytic process. These data are consistent with the results of the catalyst activity shown in the recycle experiments (Fig. 9).

4. Conclusions

In this work, the design and the grafting of a chiral Mn(III)-porphyrin complex for mimicking methane monooxygenase-like activity were inspired by both the structure of chiral porphyrin Mn(III) and the functional skeleton of mesoporous silica SBA-15. Nanocomposite SBA15-[Mn(TCPP-R*)Cl] showed the potential for the enantioselective epoxidation of aryl olefins with green oxidant oxygen, to produce specific enantiomers of aromatic epoxide compounds. The products of these reactions may be valuable building blocks for chiral compounds, such as (1S,2R)-indene oxide. The catalyst showed excellent enantioselectivity than it homogeneous counterpart in the oxidation of α-methylstyrene. Considering the nature of the non-toxicity of Mn(III) ions and biocompatibility of silica, SBA15-[Mn(TCPP-R*)Cl] is expected to have potential application in the green synthesis of complex chiral molecules.

Acknowledgments

The authors are grateful for the financial support of this study by the University of Zanjan and the Iran National Science Foundation under Grant No. INSF 95820950.

Appendix A. Supplementary material

Supplementary data associated with this article can be found, in the online version, at http://dx.doi.org/10.1016/j.jcat.2017.05.014.

References

[1] C.H. Senanayake, F.E. Roberts, L.M. DiMichele, K.M. Ryan, J. Liu, L.E. Fredenburgh, B.S. Foster, A.W. Douglas, R.D. Larsen, T.R. Verhoeven, P.J. Reider, Tetrahedron Lett. 36 (1995) 3993.
[2] P.J. Reider, Chimia 51 (1997) 306.
[3] X.M. O'Brien, J.A. Parker, P.A. Lessard, A.J. Sinskey, Appl. Microbiol. Biotechnol. 59 (2002) 389.
[4] N.K. Pandit, Introduction to the Pharmaceutical Sciences, Lippincott Williams-Wilkins, 2007, p. 87.
[5] M. Sono, M.P. Roach, E.D. Coulter, J.H. Dawson, Chem. Rev. 96 (1996) 2841.
[6] E. Rose, B. Andrioletti, S. Zrig, M. Quelquejeu-Ethève, Chem. Soc. Rev. 34 (2005) 573.
[7] K.M. Kadish, K.M. Smith, R. Guilard (Eds.), The Porphyrin Handbook, Academic Press, San Diego, 2000.
[8] H. Lu, X.P. Zhang, Chem. Soc. Rev. 40 (2011) 1899.
[9] C.-M. Che, V.K.-Y. Lo, C.-Y. Zhou, J.-S. Huang, Chem. Soc. Rev. 40 (2011) 1950.
[10] M.O. Senge, M. Fazekas, E.G.A. Notaras, W.J. Blau, M. Zawadzka, O.B. Locos, E.M. N. Mhuircheartaigh, Adv. Mater. 19 (2007) 2737.
[11] H.-B. Fa, L. Zhao, X.-Q. Wang, J.-H. Yu, Y.-B. Huang, M. Yang, D.-J. Wang, Eur. J. Inorg. Chem. (2006) 4355.
[12] E.A. Prasetyanto, S.E. Park, Appl. Catal. A: Gen. 350 (2008) 244.
[13] M.B. Yue, L.B. Sun, Y. Cao, Z.J. Wang, Y. Wang, Q. Yu, J.H. Zhu, Micropor. Mesopor. Mater. 114 (2008) 74.
[14] X.G. Wang, K.S.K. Lin, J.C.C. Chan, S. Ch-eng, J. Phys. Chem. B 109 (2005) 1763.
[15] T. Ressler, U. Dorn, A. Walter, S. Schwarz, A.H.P. Hahn, J. Catal. 275 (2010) 1.
[16] M. Alvaro, A. Corma, D. Das, V. Fornés, H. García, Chem. Commun. (2004) 956.
[17] D.E.D. Vos, M. Dams, B.F. Sels, P.A. Jacobs, Chem. Rev. 102 (2002) 3615.
[18] E. Rose, M. Soleilhavoup, L. Christ-Tommasino, G. Moreau, J.P. Collman, M. Quelquejeu, A. Straumanis, J. Org. Chem. 63 (1998) 2042.
[19] M.A. Schiavon, L.S. Iwamoto, A.G. Ferreira, Y. Iamamoto, M.V.B. Zanoni, M.das D. Assis, J. Braz. Chem. Soc. 11 (2000) 458.
[20] H.U. Blaser, Chem. Commun. (2003) 293.
[21] S. Alavi, H. Hosseini-Monfared, M. Siczek, J. Mol. Catal. A: Chem. 377 (2013) 16.
[22] R. Srivastava, D. Srinivas, P. Ratnasamy, J. Catal. 233 (2005) 1.
[23] S. Alavi, H. Hosseini-Monfared, P. Aleshkevych, RSC Adv. 4 (2014) 48827.
[24] D. Khvostichenko, Q.Z. Yang, R. Boulatov, Angew. Chem., Int. Ed. 46 (2007) 8368.
[25] I. Remsen, Am. Chem. J. 24 (1900) 52.
[26] F.L. Benedito, S. Nakagaki, A.A. Saczk, P.G. Peralta-Zamorab, C.M.M. Costa, Appl. Catal. A. 250 (2003) 1.
[27] W. Xie, L. Hu, X. Yang, Ind. Eng. Chem. Res. 54 (2015) 1505.
[28] E.Y. Jeong, M.B. Ansari, Y.H. Mo, S.E. Park, J. Hazard. Mater. 185 (2011) 1311.
[29] Q. Peng, Y. Yang, Y. Yuan, J. Mol. Catal. A: Chem. 219 (2004) 175.
[30] J.H. Shi, Q. Zhang, W.Y. Liu, M. Yu, Solid State Sci. 13 (2011) 1102.
[31] F.B. Zanardi, I.A. Barbosa, P.C. de Sousa Filho, L.D. Zanatta, D.L. da Silva, O.A. Serra, Y. Iamamoto, Micropor. Mesopor. Mater. 219 (2016) 161.
[32] R.F. Pasternack, P.R. Huber, P. Boyd, G. Engasser, L. Francesconi, E. Gibbs, P. Fasella, G.C. Venturo, L. deC. Hinds, J. Am. Chem. Soc. 94 (1972) 4511.
[33] K. Kano, M. Takei, S. Hashimoto, J. Phys. Chem. 94 (1990) 2181.
[34] K.Y. Lee, Y.S. Lee, S. Kim, H.M. Ha, S.-E. Bae, S. Huh, H.G. Janga, S.J. Lee, CrystEngComm 15 (2013) 9360.
[35] X. Feng, G.E. Fryxell, L.-Q. Wang, A.Y. Kim, J. Liu, K.M. Kemner, Science 276 (1997) 923.

[36] X. Zhang, X. Liu, J. Peng, Y. Zhao, Q. Yang, Catal, Sci. Technol. 4 (2014) 1012.
[37] D.L. Hughes, G.B. Smith, J. Liu, G.C. Dezeny, C.H. Senanayake, R.D. Larsen, T.R. Verhoeven, P.J. Reider, J. Org. Chem. 62 (1997) 2222.
[38] R.R. Diaz, K. Selby, D.J. Waddington, J. Chem. Soc., Perkin Trans. 2 (1975) 758.
[39] M. Okumura, S. Tsubota, M. Haruta, J. Mol. Catal. A 199 (2003) 73.
[40] P.E. Boahene, K.K. Soni, A.K. Dalai, J. Adjaye, Appl. Catal. A Gen. 402 (2011) 31.
[41] Z. Lei, L. Gao, H. Shui, W. Chen, Z. Wang, S. Ren, Fuel Process. Technol. 92 (2011) 2055.
[42] X. Zhou, X. Yu, J. Huang, S. Li, L. Li, C. Che, Chem. Commun. (1999) 1789.
[43] C. Li, H. Zhang, D. Jiang, Q. Yang, Chem. Commun. (2007) 547.